Effects of neodymium incorporation on the structural and luminescence properties of the $YAl_3(BO_3)_4$–$NdAl_3(BO_3)_4$ system

2007 J. Phys.: Condens. Matter 19 246204

(http://iopscience.iop.org/0953-8984/19/24/246204)

IOP PUBLISHING JOURNAL OF PHYSICS: CONDENSED MATTER

J. Phys.: Condens. Matter **19** (2007) 246204 (13pp) doi:10.1088/0953-8984/19/24/246204

Effects of neodymium incorporation on the structural and luminescence properties of the $YAl_3(BO_3)_4$–$NdAl_3(BO_3)_4$ system

A Benayas[1], D Jaque[1], J García Solé[1], N I Leonyuk[2], E Bovero[3], E Cavalli[3] and M Bettinelli[4]

[1] GIEL, Departamento de Física de los Materiales, Facultad de Ciencias, Universidad Autónoma de Madrid, Madrid 28049, Spain
[2] Department of Crystallography and Crystallochemistry, Geological Faculty, Moscow State University, 119992/GSP-2 Moscow, Russia
[3] Dipartimento di Chimica Generale ed Inorganica, Chimica Analitica e Chimica Fisica, Università di Parma, viale GP Usberti 17/a, 43100 Parma, Italy
[4] Dipartimento Scientifico e Tecnologico, University of Verona and INSTM, UdR Verona, Ca' Vignal, Strada Le Grazie 15, 37134 Verona, Italy

Received 7 February 2007, in final form 23 April 2007
Published 17 May 2007
Online at stacks.iop.org/JPhysCM/19/246204

Abstract

The luminescence of Nd^{3+} ions in $Nd_xY_{1-x}Al_3(BO_3)_4$ (Nd:YAB) single crystals has been investigated as a function of the neodymium concentration in order to evidence the relation between the structural and spectroscopic properties in this nonlinear laser system. The analysis of the experimental data allowed us to individuate four different composition ranges. For moderate concentrations ($x < 0.2$) the lattice parameters are nearly constant, and the emission spectra arise from Nd^{3+} ions in unperturbed crystal sites. For concentrations in the $0.2 < x < 0.75$ range the lattice parameters notably depend on the neodymium content, and a concomitant variation of the luminescence features is observed. In the $0.75 < x < 0.9$ range a hexagonal to monoclinic phase transition takes place: the structural disorder is evidenced well by the broadening of the emission lines and by discontinuities in the concentration behaviour of other indicators such as the crystal-field strength, energy transfer parameters, etc. Finally, for $x > 0.9$ the final formation of the $NdAl_3(BO_3)_4$ (NAB) monoclinic phase is complete, and a new local ordering around Nd^{3+} is very evident in the spectral features.

1. Introduction

Neodymium-doped yttrium aluminium borate crystals ($Nd_xY_{1-x}Al_3(BO_3)_4$, hereafter Nd:YAB) have been extensively studied in the past because of their potential applications in the field of solid-state lasers. When the neodymium content is below 5 at.% ($x < 0.05$) the excellent nonlinear properties of the YAB matrix combine with the advantageous spectroscopic

properties of Nd^{3+} ions (high emission cross section, high absorption cross section and absence of excited-state absorption at laser wavelengths) [1], giving rise to active media suitable for efficient self-frequency-doubling and self-frequency-sum-mixing laser systems capable, for example, of simultaneous multi-frequency conversion in the three fundamental colours [2, 3]. In this material the neodymium concentration can be increased up to 100%, yielding the fully concentrated neodymium aluminium borate crystal (NAB). At variance with most neodymium stoichiometric crystals, NAB shows unexpected good spectroscopic properties (longer fluorescence lifetime and reduced fluorescence bandwidth) which allow for efficient laser oscillation in the infrared [4]. Additionally, its large absorption coefficients (above 100 cm^{-1} at 808 nm) [4] provides the possibility of developing efficient microchip laser devices capable of short pulse generation and single-mode laser oscillation [5, 6]. Unfortunately, such high neodymium concentration decreases the nonlinear response of the system and multi-frequency laser oscillation based on intracavity wave mixing processes is not possible for NAB lasers. In this way, the use of 'moderately' doped Nd:YAB crystals, combining nonlinear properties and short absorption lengths, could provide the possibility of microchip multi-frequency laser systems. In this sense it is very important to have detailed information about the effects of the composition on the spectroscopic and structural properties of Nd:YAB.

Another interesting aspect is connected to the fact that YAB and NAB crystals have different structural properties. YAB belongs to the hexagonal system [7], whereas NAB is monoclinic [8]. In previous studies concerning $Nd_xY_{1-x}Al_3(BO_3)_4$ powders synthesized by solid-state reaction, x-ray diffraction experiments provided evidence that the hexagonal to monoclinic phase transition occurs when the neodymium concentration exceeds 80% (i.e. for $0.8 < x < 0.9$) [9]. Nevertheless, this structural phase transition has not been yet studied in single crystals. Furthermore, the possible influence of this structural phase transition on the luminescence properties of Nd^{3+} ions is still unexplored.

In this work we have systematically studied the structural and the luminescence properties of $Nd_xY_{1-x}Al_3(BO_3)_4$ single crystals (with x ranging from 0.01 up to 1) in order to investigate how the crystal field surrounding the Nd^{3+} ions and the excited-state dynamics are affected by the Nd^{3+} content and by the YAB–NAB structural phase transition. At the same time, the analysis of the Nd^{3+} luminescence properties have been used to extract information about how the incorporation of Nd^{3+} affects the $Nd_xY_{1-x}Al_3(BO_3)_4$ lattice, in such a way that the neodymium ions are used as optical probes.

The paper is organized as follows. In section 2 the experimental procedures for the crystal growth and the spectroscopic measurements are described. Section 3 is dedicated to the presentation of the experimental results: in section 3.1 the effect of the composition (x) on the lattice parameters and crystal structure will be discussed on the basis of the x-ray diffraction measurements. In section 3.2 we will examine the effect of the neodymium concentration on the characteristics of the $^4F_{3/2} \rightarrow {}^4I_{11/2}$ emission channel. In section 3.3 the decay profiles of this luminescence are analysed and the relative contribution of the different energy transfer mechanisms and their dependence on the Nd^{3+} concentration are assessed. Finally, in section 4 we summarize the main conclusions obtained from this work.

2. Experimental details

2.1. Crystal growth and structural data

The $Nd_xY_{1-x}Al_3(BO_3)_4$ ($0.01 \leqslant x \leqslant 1$) crystals were grown by the flux growth method, using $K_2Mo_3O_{10}{\cdot}B_2O_3$ as a solvent. Reagent-grade K_2CO_3 (Carlo Erba) and H_3BO_3 (Merck), 99.5% MoO_3 (Aldrich), and 99.99% Y_2O_3 (Aldrich) and 99.99% Nd_2O_3 (Riedel de Haën)

were used as starting materials. The growth mixture was put into a platinum crucible and heated to 1200 °C at a rate of 60 °C h^{-1} in a horizontal furnace. After a 6 h soaking time the temperature was lowered to 700 °C at a rate of 1.2 °C h^{-1}, and then to room temperature at a rate of 15 °C h^{-1}. Good optical-quality crystals with a size of about $1 \times 1 \times 3$ mm^3 were obtained. We have verified, by means of x-ray fluorescence analysis, that the actual Nd^{3+} content coincides with the nominal one in the whole concentration range.

For each neodymium concentration the cell parameters as well as the corresponding structural phase have been determined from the analysis of the x-ray diffraction patterns obtained from single crystals with a four-circle P4 Siemens diffractometer.

2.2. Spectroscopy measurements

For continuous-wave (CW) luminescence spectra a 0.6 W fibre coupled diode tuned to 807 nm was used as the excitation source. The emission experiments under pulsed excitation were performed by exciting the sample with an optical parametric oscillator (OPO Quanta Ray) which provides 10 ns pulses with an average energy of 10 mJ. The OPO wavelength was tuned between 870 and 900 nm with a spectral resolution better than 0.1 nm. In both CW and pulsed excitation experiments the luminescence was dispersed by a half metre spectrometer (SPEX 500 M) and detected with a calibrated Ge detector or a cooled photomultiplier. The spectral resolution around 1.06 μm was below 0.1 nm. In CW luminescence experiments the signals were recorded by using an EG&G lock-in amplifier. Decay time measurements were recorded by a LeCroy digital storage oscilloscope. The uncertainty in lifetime measurements was around 5%. Low-temperature (15 K) experiments were performed by mounting the samples in a Leybold temperature-controlled closed-cycle He cryostat.

3. Results and discussion

3.1. Structural data and x-ray diffraction experiments

YAB belongs to the hexagonal system, space group $R32$, with cell parameters $a = b = 9.295$ Å and $c = 7.243$ Å ($Z = 3$) [10]. In YAB crystals Nd^{3+} replaces Y^{3+} in sites coordinating six oxygen ions located at distances of 2.321 Å and forming distorted trigonal prisms with D_3 point symmetry. The shortest Y(Nd)–Y(Nd) distance is 5.88 Å, each Y^{3+} (Nd^{3+}) ion being surrounded by six other ones at that distance. On the other hand, NAB is a polymorphous compound presenting three crystal structures (α and β both monoclinic and γ hexagonal) and two phase transitions ($\alpha \rightarrow \beta$ at 922 °C and $\beta \rightarrow \gamma$ at 1016 °C) [11]. The best-known form is β-NAB, whose space group is $C2/c$ with cell parameters $a = 7.262$ Å, $b = 9.365$ Å and $c = 11.138$ Å with $\beta = 103.4°$ ($Z = 4$). In β-NAB crystals the coordination polyhedron around Nd^{3+} is distorted with respect to that described above for Nd:YAB crystals. It consists of six oxygen ions, four of which are located at 2.382 and two at 2.399 Å. The actual point symmetry is C_2, although the D_3 geometry also represents a reasonable approximation. In the case of β-NAB the separation distances between one Nd^{3+} ion and its two and four closest Nd^{3+} neighbours are 5.60 and 5.91 Å, respectively [11]. The structures of YAB and β-NAB are relatively similar: the latter can be, in fact, considered as generated by the former through a deformation of the primitive rhombohedral cell.

The lattice parameters, as well as the crystalline phases, of all the crystals under investigation have been determined from room-temperature x-ray diffraction measurements. We have found that the expected hexagonal to monoclinic structural phase transition is complete when the neodymium content exceeds 0.9, in rather good agreement with previous studies [9]. In figure 1 the values of lattice parameters are reported as a function of x in the concentration range corresponding to the hexagonal (Nd:YAB) phase. The lattice parameters obtained for

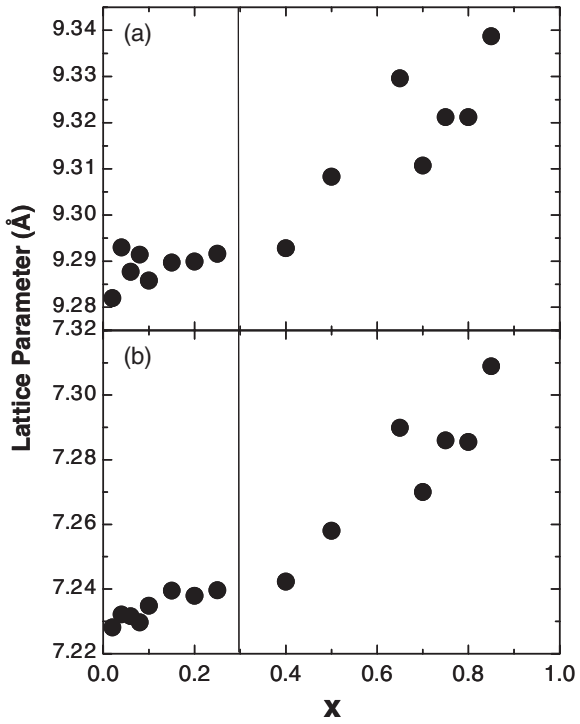

Figure 1. *a* (a) and *c* (b) lattice parameters as a function of the Nd^{3+} content (x) in the concentration range corresponding to the hexagonal (YAB) phase.

compositions above $x = 0.9$ (i.e. above the structural phase transition) have been found, within experimental error, to be independent of the x content. Furthermore, we have only two different x contents in this range, so the observation of a trend is difficult. The continuous increase of the lattice constants observed in figure 1 for Nd:YAB crystals can be ascribed to the larger ionic radius of Nd^{3+} (0.98 Å) with respect to Y^{3+} (0.90 Å) [12]. At variance with the data of [9], figure 1 evidences a negative deviation from the Vegard's law (which assumes a linear relationship between the substitutional impurity concentration and the lattice parameter). Indeed, from the data of figure 1 two different increment rates can be elucidated; for $x < 0.3$ the lattice parameters increase slightly with the neodymium content, whereas for $x > 0.3$, the increase of the lattice parameters with the Nd^{3+} concentration is much more pronounced. Thus, the data included in figure 1 show the existence of a relevant influence of the Nd^{3+} content in the local properties of the Nd:YAB system even for Nd^{3+} contents far away from those required for the structural phase transition. Since the spectroscopic features of the rare-earth ions are certainly affected by concentration effects and by local perturbations of the crystal field, in the following sections we will investigate the emission properties of the Nd:YAB system as a function of the composition in order to obtain further information about the relation between crystallographic and spectroscopic properties.

3.2. Emission spectra

Figure 2 shows the room-temperature unpolarized emission spectra corresponding to the $^4F_{3/2} \rightarrow {}^4I_{11/2}$ transition obtained for different Nd^{3+} contents after 808 nm excitation

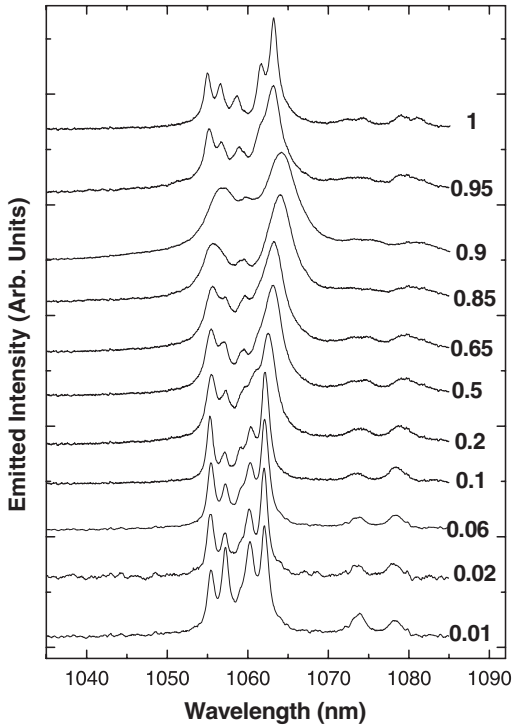

Figure 2. Room-temperature emission spectra corresponding to the $^4F_{3/2} \rightarrow {}^4I_{11/2}$ transition obtained for different Nd^{3+} contents after 808 nm excitation ($^4I_{9/2} \rightarrow {}^4F_{5/2}$ excitation channel).

($^4I_{9/2} \rightarrow {}^4F_{5/2}$ excitation channel). Due to the broad-band nature of diode excitation, no site selection is achieved and the spectra should be representative of all the possible Nd^{3+} sites. The obtained spectra are strongly dependent on x, especially for compositions approaching the one corresponding to the phase transition ($x \approx 0.85$). In order to analyse these changes in more detail we have focused our attention on the full width at half maximum (FWHM) and on the energy position of the strongest emission line at about 1062 nm (figures 3(a) and (b), respectively). From figure 2 it is possible to distinguish four different content ranges:

- *Range I* ($x < 0.3$). In this low Nd^{3+} concentration range the FWHM value weakly increases and the energy of the main peak weakly decreases with the Nd^{3+} concentration. The broadening of the fluorescence lines gives an indication of the homogeneity of the crystal field surrounding the optical centre, whereas the peak position depends on its strength and geometry [13]. On this basis, we infer that in this concentration range the substitution of yttrium ions by neodymium ions implies minor perturbations of the local geometry of the active centre. This behaviour is consistent with the slight variation of the lattice parameters observed in this range (see figure 1).
- *Range II* ($0.3 < x < 0.75$). In this concentration range both the FWHM and peak position are strongly affected by the incorporation of neodymium ions. The increase of inhomogeneous broadening can be ascribed to perturbations in the crystal field induced by the incipient modification of the crystal structure and by the increasing presence of Nd^{3+} ions in the second coordination sphere of the optical centre, leading, among others, to the formation of Nd–Nd pairs, clusters, etc. The shift of the peak position to lower energies

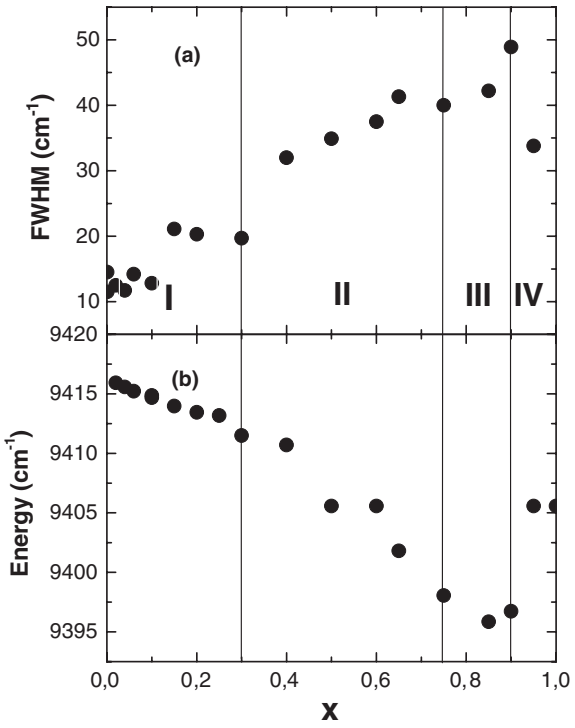

Figure 3. (a) Full width at half maximum (FWHM) and (b) energy position of the strongest emission line within the $^4F_{3/2} \rightarrow {}^4I_{11/2}$ fluorescence band at 1062 nm as a function of the Nd^{3+} content (x).

confirms alterations in the local geometry around Nd^{3+} ions. As can be observed from figure 1, this behaviour coincides with a strong dependence of the lattice constants on the Nd^{3+} content.

- *Range III* ($0.75 < x < 0.9$). In this third range the fluorescence broadening and the shift of the peak energy have reached their limit values and do not change any further with the increase of the Nd^{3+} content. This range corresponds to the structural phase transition, so the $Nd_xY_{1-x}Al_3(BO_3)_4$ system has attained its maximum structural disorder and the emission properties are nearly independent of the Nd^{3+} content. In this range the spectroscopic properties are more similar to those of a glass than of a crystal.
- *Range IV* ($0.9 < x < 1$). In this concentration range the structural phase transition has already occurred, inducing a strong reordering in the Nd^{3+} local environment. This accounts for the reduction of the emission linewidth. At the same time, the main line shifts back towards high energies. The spectral linewidth of the $^4F_{3/2} \rightarrow {}^4I_{11/2}$ transition in the NAB system is, in fact, comparable to that of diluted Nd:YAB crystals, indicating in both cases a high homogeneity of the crystal field.

  In order to obtain further information about the dependence of the crystal field on the Nd^{3+} content, we have recorded the 15 K excitation spectra of all the crystals in the $^4I_{9/2} \rightarrow {}^4F_{3/2}$ spectral region. Figure 4 shows, as an example, the $^4I_{9/2} \rightarrow {}^4F_{3/2}$ excitation spectrum obtained for $x = 0.02$ (the emission wavelength in this case was 1.06 μm). It consists of two peaks at $E_1 \approx 11\,390$ cm^{-1} and $E_2 \approx 11\,440$ cm^{-1}, corresponding to the transitions usually called $1 \rightarrow R_1$ (E_1) and $1 \rightarrow R_2$ (E_2) respectively, where 1 denotes the

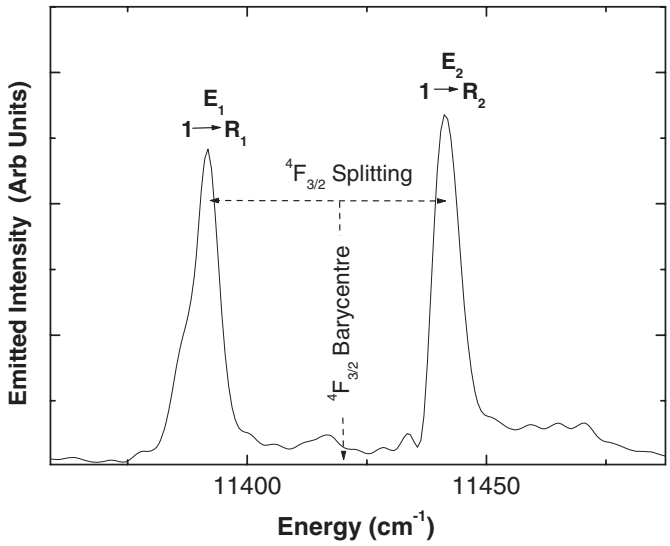

Figure 4. Low-temperature $^4I_{9/2} \rightarrow {}^4F_{3/2}$ excitation spectrum obtained for $x = 0.02$ (the emission wavelength in this case was 1.06 μm).

lowest energy sublevel (0 cm^{-1}) of the $^4I_{9/2}$ ground state and R_1 and R_2 are the two Stark components of the $^4F_{3/2}$ state [14]. It is then possible, from the low-temperature excitation spectra, to calculate both the energy splitting ($E_2 - E_1$) and energy barycentre ($\frac{E_2+E_1}{2}$) of the $^4F_{3/2}$ emitting state for all the crystals under investigation. The results are shown in figures 5(a) and (b). Again, the behaviour of both quantities with the composition can be rationalized on the basis of the four ranges previously defined.

- In *range I* ($x < 0.3$) the barycentre of the $^4F_{3/2}$ level is nearly constant, whereas its splitting slightly increases. Thus, we can deduce that in this range the crystal-field strength around the Nd^{3+} ions moderately increases with the Nd^{3+} content. In addition we can also conclude, from the invariance of the of the $^4F_{3/2}$ barycentre, that, in this concentration range, the covalence of the Nd–O bond is unchanged, i.e. the nephelauxetic effect is negligible in this concentration range [15, 16].
- In *range II* ($0.3 < x < 0.75$) the increase of x implies a relevant increase (up to about 30 cm^{-1}) of the splitting of the $^4F_{3/2}$ level and an analogous red shift of its barycentre. This, together with the possible variation of the splitting of the terminal $^4I_{11/2}$ state, should account for the remarkable shift of the 1.06 μm peak displayed in figure 2. The relevant variations with x observed in the splitting and barycentre of the $^4F_{3/2}$ state indicate that the local structure around the Nd^{3+} ions is being modified [13]. In particular, the increase of the crystal-field strength and the red shift of the barycentre seem to indicate that the Nd–O bonds are undergoing an effective compression as x increases, this leading to an increment in the crystal-field strength as well as in the covalence of the Nd–O bonds [13, 15, 16]. At this point it is important to note that the 0.75 content is a borderline content lying between the regimes II and III, so the 0.75 sample could show spectroscopic properties that could belong to the trends associated to either of those regimes (II and III). This could explain the fact that the $^4F_{3/2}$ barycentre value obtained for the 0.75 sample agrees with the trend corresponding to the regime II whereas that found for the $^4F_{3/2}$ splitting seems to be more in accordance with the trend associated to regime III.

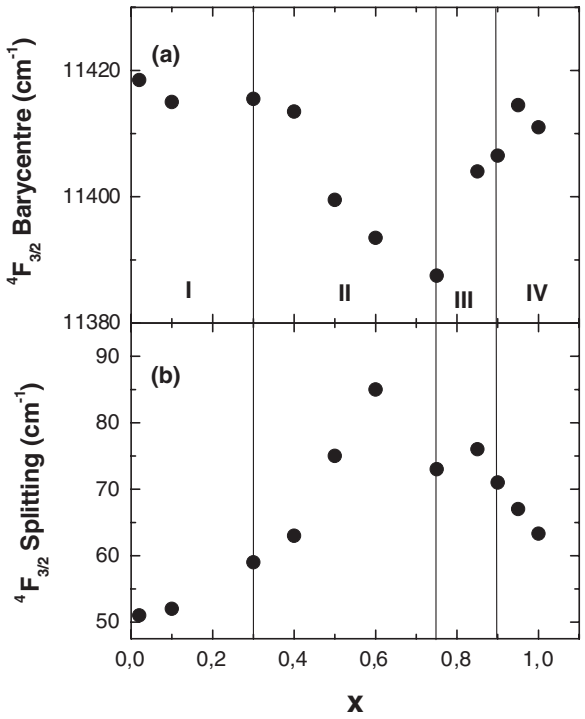

Figure 5. (a) Energy splitting and (b) barycentre of the $^4F_{3/2}$ metastable state of Nd^{3+} ions as a function of the Nd^{3+} content (x).

- *Range III* ($0.75 < x < 0.9$) corresponds to the onset of the phase transition and to the maximum structural disorder: the $^4F_{3/2}$ splitting and barycentre do not vary with x, as well as the line width and position of the 1.06 μm peak (see figure 3).
- Finally, in *range IV* ($0.9 < x < 1$), the system has undergone the structural phase transition to the monoclinic structure. The decrease in the $^4F_{3/2}$ splitting with x (see figure 5(b)) indicates a decrease in the strength of the crystal field around the Nd^{3+} ions. On the other hand, the $^4F_{3/2}$ barycentre slightly shifts to higher energies (figure 5(a)) with Nd^{3+} content, probably accounting for the long Nd–O distances typical of the NAB structure [10, 11]. The combination of these effects leads to the back-shift towards higher energies of the 1.06 μm peak position in this compositional range (see figure 3(b)).

3.3. Time-resolved luminescence experiments

Data arising from CW experiments clearly reveal that the increase of the Nd^{3+} concentration progressively affects the geometry around the Nd^{3+} ions, introducing a structural disorder that reaches its maximum for the composition corresponding to the structural phase transition. These changes in the local environment could also account for relevant modifications in the strength and nature of the Nd^{3+}–Nd^{3+} interactions that could induce changes in the non-radiative probability associated to the relaxation of the $^4F_{3/2}$ metastable state. In order to verify this possibility, we have measured the decay curves of the 1.06 μm luminescence following pulsed excitation at 890 nm ($^4I_{9/2} \rightarrow {}^4F_{3/2}$ transition). Figure 6 shows that the decay profiles clearly depend on the composition. Up to x values of the order of 0.1, the curves are single

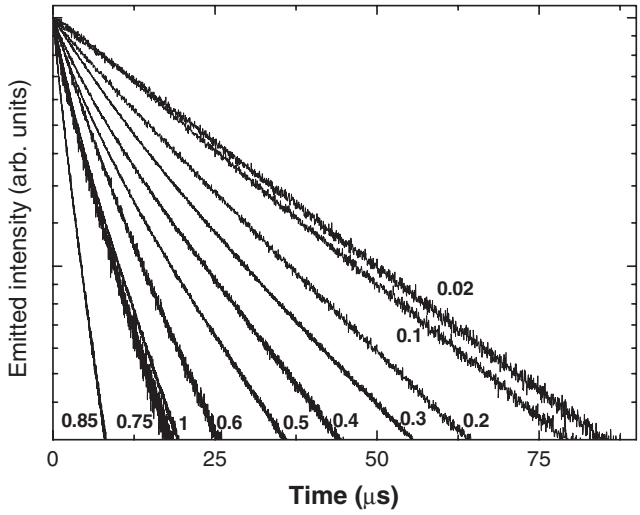

Figure 6. Room temperature fluorescence decay curves of the $^4F_{3/2}$ state obtained for different Nd^{3+} contents.

exponential. When x exceeds 0.1, the decays deviate from the exponential behaviour, mainly at short times after excitation. The fluorescence decay becomes faster as the x content increases (i.e. the $^4F_{3/2}$ fluorescence lifetime decreases with the Nd^{3+} content). This trend continues until $x = 0.9$; then the decay times increase as the neodymium content is increased, in contrast with the behaviour generally observed in highly or fully Nd^{3+} concentrated crystals, whose luminescence is usually affected by a strong concentration quenching [13]. Both the experimental decay profiles and the concentration dependence of the decay rate can be described within the framework of the donor–acceptor transfer theory developed for singly doped crystals [17–28]. According to this theory, the processes responsible for the increase of the non radiative decay rate mainly consist of excitation transfers from a donor ion (Nd^{3+} in an excited state) to an acceptor centre (Nd^{3+} in the ground state and/or luminescence traps or killer centres). The resulting decay profile strongly depends on whether this transfer occurs in presence or in absence of energy migration among the donors, and therefore on the neodymium concentration. There are two limiting cases.

(i) *Static case*: the donor–acceptor energy transfer rate is much higher than the migration rate, i.e. migration can be neglected. The non-radiative decay rate is strongly time dependent and the fluorescence decay curve is non-exponential at short times. At long times the decay profile tends to the exponential behaviour of the isolated donor ions. For an electric dipole–electric dipole interaction between donor and acceptor, the time dependence of the luminescence after pulsed excitation at $t = 0$ is given by [17, 18, 22–28]

$$I(t) = I_0 \exp -\left[\frac{t}{\tau_0} + \gamma_{dd} t^{1/2}\right] \tag{1}$$

where τ_0 is the intrinsic lifetime of Nd^{3+} ions (i.e. the fluorescence lifetime of diluted Nd:YAB crystals) and γ_{dd} is a time-independent parameter.

(ii) *Dynamic case*: the donor–acceptor energy transfer occurs in the presence of fast-energy migration between donors. The non-radiative decay rate is constant for all the times after excitation, since in this limit case the energy migration favours energy transfer between one

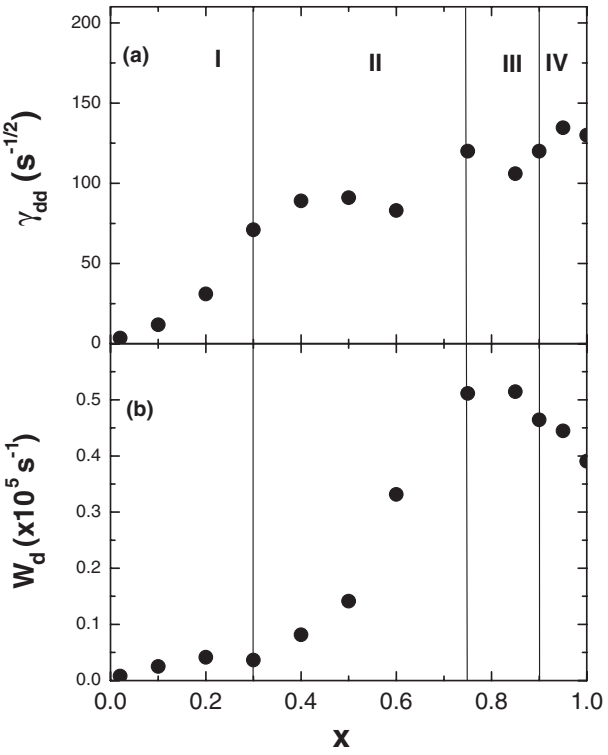

Figure 7. γ_{dd} (a) and W_d (b) time-independent parameters as a function of the Nd^{3+} content (x).

donor and the closest acceptor. The decay profile of the luminescence is given by [17–22]:

$$I(t) = I_0 \exp - \left[\frac{t}{\tau_0} + W_d t \right] \tag{2}$$

where W_d and τ_0 are time-independent constants.

In the most general case both static and migration-assisted donor–acceptor energy transfer processes take place simultaneously, and the time decay of the fluorescence can be described by [29]

$$I(t) = I_0 \exp - \left[\frac{t}{\tau_0} + \gamma_{dd} t^{1/2} + W_d t \right]. \tag{3}$$

The decay curves of figure 6 have been fitted to expression (3) in order to estimate how the relative contributions of static and dynamic processes vary with the crystal composition. The results of the fit are shown in figure 7, where the γ_{dd} and W_d time-independent parameters are plotted as a function of the Nd^{3+} content. In the calculation of these two parameters we have assumed a concentration-independent intrinsic lifetime of 53 μs, as provided by [1]. Of course this is a rough approach since the concentration dependence of the exponential contribution (i.e. of the $\frac{1}{\tau_0} + W_d$ term) to the fluorescence decay curves is completely associated to concentration-induced changes in the W_d parameter (i.e. the $\frac{1}{\tau_0}$ is assumed to be concentration independent). In this way the possible concentration dependence of the intrinsic lifetime has not been considered. We point out that γ_{dd} represents the total energy transfer parameter, and takes into account the cross relaxation in regular Nd^{3+} centres and the transfer to killer centres. Once again the existence of four concentration ranges is clearly observed:

(i) *Range I.* The donor–acceptor transfer rate γ_{dd} significantly increases with the Nd^{3+} content, whereas W_d, the migration rate, is low and nearly constant. This behaviour is consistent with the progressive reduction of the Nd–Nd distances in a concentration region where the density of the active centres is too low to give rise to appreciable migration processes.

(ii) *Range II.* In this range both W_d and γ_{dd} increase with the Nd^{3+} content. However, the concentration dependence of γ_{dd} is less pronounced than in the low-concentration range, whereas the migration rate rapidly grows up to a maximum value in correspondence of $x = 0.75$. This strong enhancement in the W_d parameter can be ascribed to the relevant reduction of the average distance between the active ions, leading, among other things, to the formation of Nd–Nd pairs and clusters with high cross-relaxation and energy-diffusion probabilities. In addition the broadening of emission bands observed in this range (see figure 2) could also indicate the presence of a high concentration of defects which could act as luminescence killers, increasing in this way the γ_{dd} parameter.

(iii) *Range III.* In the region corresponding to the phase transition the static and migration-assisted donor–acceptor energy transfer rates have their largest values and are practically concentration independent. The structural disorder, implying the broadening of the absorption and emission features, and the high density of active centres account for the observed behaviour.

(iv) *Range IV.* After the formation of the monoclinic phase the γ_{dd} parameter tends again to increase slightly with the Nd^{3+} content, whereas W_d tends to decrease. We infer that the donor–acceptor transfer is still favoured by concentration effect, whereas the migration is affected by the increase of the distances between the Nd^{3+} centres, typical of the NAB structure with respect to the YAB one [7, 8].

In the presence of both static and dynamic energy transfer mechanisms the storage capability of the $4F_{3/2}$ state is determined by the average fluorescence decay time, τ_{av}, which can be expressed as

$$\tau_{av} = \frac{\int I(t) \cdot t \, dt}{\int I(t) \, dt}. \tag{4}$$

Figure 8 reports the average fluorescence decay time as a function of the Nd^{3+} content obtained from the experimental decay profiles. In range I, when the migration is nearly absent, the decay time rapidly decreases with the concentration. The slope is less pronounced in range II, where the effects of the migration and of the structural disorder become more and more important. In correspondence with the phase transition (range III), the value of τ_{av} is stabilized to a minimum value, and after the formation of the monoclinic phase it tends again to increase. From the comparison with the data of figure 7 it can be deduced that the donor–acceptor transfer plays a more important role than the migration in determining the fluorescence decay time, and hence the fluorescence quantum efficiency, of the $^4F_{3/2}$ metastable state. This point of view is supported by structural considerations, since the Nd^{3+} (Y^{3+}) polyhedra are well separated from each other by BO_3^{3-} and AlO_6^{6-} units (minimum separation distances of the order of 5.9 Å in YAB and 5.6 and 5.9 Å in NAB). It can also be pointed out that the migration (followed by transfer to killer centres) is considered to be responsible for the strong (often complete) quenching of the luminescence usually observed in crystals containing high concentrations of Nd^{3+} ions [13]. In the present case the quenching is relatively far from being complete, thanks to the limited effects of the migration processes once the structural phase transition has been overcome. In absence of this phase transition a complete (or at least severe) luminescence quenching was expected for a Nd^{3+} content of 0.85 (see the extrapolated solid

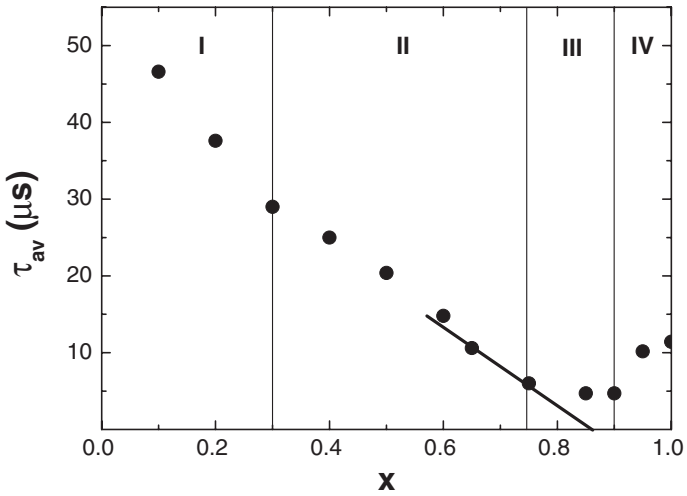

Figure 8. $^4F_{3/2}$ average fluorescence decay time as a function of the Nd^{3+} content (x).

line in figure 8). This is in fact an outstanding feature when compared with other neodymium stoichiometric crystals, in which the Nd^{3+} concentrations are accompanied by a strong donor–acceptor energy transfer which leads to typical fluorescence lifetimes below 1 μs [30].

4. Conclusions

We have investigated the luminescence and structural properties of $Nd_xY_{1-x}Al_3(BO_3)_4$ system with Nd^{3+} contents varying in a full concentration range between $x = 0.02$ (diluted Nd:YAB crystals) and $x = 1$ (NAB stoichiometric crystals). The analysis of the data obtained from emission measurements carried out at room and low temperature upon CW and pulsed excitation allowed us to individuate a number of independent parameters closely connected to the local structure around the active centres inside the crystal. All these parameters vary with the Nd^{3+} content following the same general behaviour. In this context, the evolution of the hexagonal to monoclinic phase transition taking place with the progressive increment of the neodymium concentration implies four well-defined concentration ranges. When $x < 0.3$ the structural properties of the YAB host are effectively conserved and the optical centres are relatively isolated one from another and maintain their original coordination geometry. For $0.3 < x < 0.75$ both lattice parameters and emission features are strongly sensitive to the concentration, evidencing a progressive structural disorder. For $0.75 < x < 0.9$ the hexagonal to monoclinic structural phase transition takes place, leading to a metastable structural state between YAB and NAB in which the local environment of Nd^{3+} ions is found to be independent of the composition x. Finally, for $x > 0.9$ the system has definitely assumed the NAB structure, and the emission features are consistent with a new ordered crystalline phase. In conclusion, Nd^{3+} has been demonstrated to be an extremely sensitive probe to follow the evolution of the structural properties of the Nd:YAB system with composition. The results presented in this work can be of interest for the optimization of multi-functional solid-state lasers based on $Nd_xY_{1-x}Al_3(BO_3)_4$. In fact it has been demonstrated that local effects caused by compositional changes have a remarkable influence on the spectroscopic parameters of relevance in laser dynamics, such as the fluorescence lifetime of the emitting state and the splitting and shape of the emission band associated to the laser transition.

Acknowledgments

The authors are grateful to Professor Gianluca Calestani (Università di Parma) for helpful discussion concerning the crystallographic properties of Nd:YAB. This work has been carried out with the financial contribution of the Italian Ministry for the University and Scientific Research (Progetto PRIN 2005).

References

[1] Jaque D, Capmany J, Luo Z D and García Solé J 1997 *J. Phys.: Condens. Matter* **9** 9715
[2] Jaque D, Capmany J and García Solé J 1999 *Appl. Phys. Lett.* **75** 325
[3] Jaque D, Capmany J and García Solé J 1999 *Appl. Phys. Lett.* **74** 1788
[4] Jaque D, Enguita O, García Solé J, Jiang A D and Luo Z D 2000 *Appl. Phys. Lett.* **76** 2176
[5] Luo Z D, Huang Y D, Montes M and Jaque D 2004 *Appl. Phys. Lett.* **85** 715
[6] Bovero E, Luo Z D, Huang H Y, Benayas A and Jaque D 2005 *Appl. Phys. Lett.* **87** 211108
[7] Wang P, Dawes J M, Dekker P, Knowles D S, Piper J A and Lu B 1999 *J. Opt. Soc. Am.* B **16** 63
[8] Xue D and Zhang S 1996 *J. Phys.: Condens. Matter* **8** 1949
[9] Jung S T, Yoon J T and Cheng S J 1996 *Mater. Res. Bull.* **31** 1021
[10] Belokoneva E I, Azivov A V, Lenyuk N I, Simonov M A and Belov N V 1981 *Zh. Struk. Khim.* **22** 196
[11] Belokoneva E I, Simonov N A, Pashkova A V, Timchenko T I and Belov N V 1980 *Sov. Phys.—Dokl.* **25** 948
[12] Shannon R D 1976 *Acta Crystallogr.* A **32** 751
[13] Henderson B and Imbusch G F 2006 *Optical Spectroscopy of Inorganic Solids* (New York: Oxford University Press)
[14] Jaque D, Enguita O, Caldiño U, Ramírez M O, García Solé J, Zaldo C, Muñoz-Santiuste J E, Giang J and Luo Z D 2001 *J. Appl. Phys.* **90** 561
[15] Biernacki S W, Kaminska A, Suchocki A and Arizmendi L 2002 *Appl. Phys. Lett.* **81** 442
[16] Reisfeld R and Boehm L 1975 *J. Non-Cryst. Solids* **17** 209
[17] Voronko Y K, Mamedov T G and Osiko V V 1976 *J. Exp. Theor. Phys.* **71** 252
[18] Sakun V P 1972 *Phys. Solid State* **14** 1906
[19] Burstein A I 1983 *J. Exp. Theor. Phys.* **84** 6
[20] Burstein A I and Sakun V P 1983 *Chem. Phys. Lett.* **103** 205
[21] Vugmeister B E 1983 *Phys. Solid State* **25** 2796
[22] Kushida T 1973 *J. Phys. Soc. Japan* **34** 1318
[23] Forster Th 1978 *Ann. Phys., Lpz.* **2** 55
[24] Forster Th 1949 *Z. Naturf.* **44** 321
[25] Dexter D I 1953 *J. Chem. Phys.* **21** 836
[26] Inokuti M and Hirayama F 1965 *J. Chem. Phys.* **43** 1978
[27] Grant J C W 1971 *Phys. Rev.* B **4** 648
[28] Martín I R, Rodriguez V D, Rodriguez-Mendoza U R, Lavin V, Montoya E and Jaque D 1999 *J. Chem. Phys.* **111** 1191
[29] Tkachuk A M, Ivanova S E, Joubert M F, Guyot Y and Guy S 2001 *J. Lumin.* **94–95** 343
[30] Majchrowski A, Michalski E and Brenier A 2003 *J. Cryst. Growth* **247** 467